Self-Assembled Monolayers of Nitrile-Functionalized Alkanethiols on Gold and Silver Substrates

S. Frey, A. Shaporenko, and M. Zharnikov*

Angewandte Physikalische Chemie, Universität Heidelberg, Im Neuenheimer Feld 253, 69120 Heidelberg, Germany

P. Harder and D. L. Allara

Departments of Chemistry and Materials Science, Pennsylvania State University, University Park, Pennsylvania 16802

Received: September 30, 2002; In Final Form: February 26, 2003

Self-assembled monolayers (SAMs) formed from nitrile-functionalized alkanethiols (AT), $NC(CH_2)_{16}SH$ (NC-C16), on (111) gold and silver substrates were characterized by X-ray photoelectron spectroscopy, near-edge X-ray absorption fine structure spectroscopy, and contact angle measurements. The average chain tilt angles in NC-C16/Ag and NC-C16/Au were estimated to be 29.5° ± 5° and 42.5° ± 5° from the surface normal, respectively, while the data suggest lower ordering for NC-C16/Au. The −C≡N bonds were found to be predominantly oriented in the surface plane with a tilt angle of 65° ± 7° for both NC-C16/Au and NC-C16/Ag. Comparison with previous data on CH_3-terminated SAMs reveals that substitution of weakly interacting CH_3 groups by the CN entities results in an increase in the average tilt angles of the alkyl chains by ∼7.5° and ∼17.5° in AT/Au and AT/Ag, respectively. A strong electrostatic interaction between the polar nitrile groups is assumed to underlie the structural behavior by controlling a balance between the headgroup−substrate and interchain interactions. The near-parallel orientation of the nitrile groups to the surface in both of these SAMs can be explained on the basis of minimization of the unfavorable CN−CN dipole−dipole interactions.

1. Introduction

During the last two decades self-assembled monolayers (SAMs) attracted considerable attention because they enable one to fabricate an organic surface of a definite chemical identity and provide a means to tailor the surfaces properties such as wetting, adhesion, lubrication, corrosion, and biocompatibility.[1−5] SAMs are polycrystalline films of chainlike or rodlike molecules that are chemically anchored to a suitable substrate. The SAM constituents consist generally of three parts: a headgroup that binds strongly to the substrate, a tailgroup that constitutes the outer surface of the film, and a spacer that connects head and tail groups. Whereas the balance between the headgroup−substrate and the intermolecular interactions is of crucial importance for the molecular structure and packing density of SAMs,[1,2,4,6−9] the identity of the tailgroup is deciding for the most of the SAM properties, providing a high orientational order and packing density in the film. A large variety of different functionalities along with a flexible molecular architecture are exactly the properties that make SAMs attractive for scientific and practical applications.

The properties of differently functionalized SAMs have been the subject of many studies. In particular, much work has been published on ω-substituted alkanethiolate (AT) SAMs on noble metal substrates, which are probably the best studied SAM systems at present because of their stability and the easiness of fabrication (e.g., see refs 10−16). However, many of these studies have concentrated on the wetting properties of SAMs formed from differently functionalized ATs and paid minor attention to the effect of the ω-substitution on the structure and packing density in these systems. Such an influence can be, however, fairly large, especially in the case in which some strongly interacting (e.g., polar groups or groups capable of hydrogen bonding) functional groups are used.[13,16] Under these conditions, the interaction between the tailgroups becomes a third participant in the structure-building interplay between the headgroup−substrate and the intermolecular forces, which can cause a significant change of the structure, orientational order, and packing density in a SAM.

In this paper, we studied SAMs formed from nitrile-functionalized alkanethiols (AT), $NC(CH_2)_{16}SH$ (NC-C16, 17-mercaptoheptadecanenitrile), on (111) gold and silver substrates. These systems are interesting from both scientific and practical standpoints. From the practical point of view, the nitrile-functionalized SAMs are perspective candidates for SAM-based lithography[17] and the fabrication of non-hydrogen-bond donor surfaces with low protein affinity.[18] From the scientific standpoint, the polar nitrile group with a relatively large dipole moment is well-suited to explore to what extent the structure of a nonsubstituted AT SAM can be affected by strongly interacting tailgroups. A theory predicts a strong influence of the electrostatic interactions between the nitrile tailgroups on the entire system.[13] A few published experimental papers concentrated on some specific issues and have not come to a clear conclusion concerning the structure of the nitrile-substituted AT SAMs,[10,19−21] even though some of the authors

* To whom correspondence should be addressed. E-mail: Michael.Zharnikov@urz.uni-heidelberg.de.

10.1021/jp0221690 CCC: $25.00
Published on Web 07/10/2003

reported a low structural order in these systems.[21] In addition, only the SAMs on Au were investigated.

We used several complementary experimental techniques, such as X-ray photoelectron spectroscopy (XPS), near-edge X-ray absorption fine structure (NEXAFS) spectroscopy, and contact angle measurements to get information on the chemical identity, packing density, and orientational and conformational order in the NC-C16 SAMs on Au and Ag. Of particular interest was the determination of the orientation of the terminal nitrile groups from the NEXAFS data. To date, the only reported example of tail group orientation by NEXAFS has involved the rather bulky phenyl tailgroups in phenyltricosanthiolate SAMs on Au.[22] As compared to the pronounced π_1* resonance of phenyl, the absorption resonances of the diatomic nitrile group have much lower intensity. Thus the nitrile SAM provides a useful test of the limits of NEXAFS spectroscopy in characterizing functionalized SAMs.

In the following section, we describe the experimental procedure and techniques. The results are presented and briefly discussed in section 3. An extended analysis of the data is given in section 4, followed by a summary in section 5.

2. Experimental Section

2.1. Synthesis of NC-C16. *17-Mercaptoheptadecanenitrile (**1**).* This compound was prepared from 16-bromohexadecan-1-ol through a nucleophilic substitution of the bromide with cyanide followed by the esterification with thiolacetic acid in the presence of diisopropyl azodicarboxylate and triphenylphosphine (Mitsunobu reaction) and finally the cleavage of the thioacetate to the thiol. All reactions were performed in a nitrogen atmosphere with A.C.S reagent grade organic solvents and deionized water. THF was freshly distilled from sodium.

*16-Bromohexadecanoic Acid (**2**).* Hexadecanolide (20 g, 78.6 mmol, Aldrich H0893) was dissolved in a mixture of 100 mL of 48% HBr and 100 mL of glacial acetic acid. The mixture was refluxed for 24 h and allowed to cool for 15 min, and the warm solution was poured into a beaker with 200 mL of cold water. The acid precipitated immediately and was filtered and washed with water until the filtrate was no longer acidic. The product on the filter was washed once with hexane, vacuum-dried, and recrystallized from 200 mL of hexane. Yield: 23.2 g (88%) 16-bromohexadecanoic acid (MW 335.3), white powder. ^{1}H NMR ($CDCl_3$): δ 3.41 (t, 2H, J = 6.9 Hz), 2.35 (t, 2H, J = 7.6 Hz), 1.85 (m, 2H), 1.63 (m, 2H), 1.42 (m, 2H), 1.37−1.22 (b, 20H).

*16-Bromohexadecan-1-ol (**3**).* The acid **2** (4.3 g, 12.8 mmol) was dissolved in 30 mL of dry THF. Thirteen milliliters of 1.5 M borane−tetrahydrofuran complex in THF (19.5 mmol, Aldrich 43,687-9) was added dropwise at 0 °C. The solution was refluxed for 24 h, cooled to room temperature, quenched with 10 mL of water, and added to a separatory funnel with 150 mL of water and 150 mL of ether. The ether phase was separated, and the aqueous phase was extracted twice with 50 mL of ether. The combined ether phases were dried with $MgSO_4$, and the solvent was evaporated under vacuum. ^{1}H NMR ($CDCl_3$): δ 3.64 (t, 2H, J = 6.6 Hz), 3.41 (t, 2H, J = 6.9 Hz), 1.86 (m, 2H), 1.57 (m, 2H), 1.44 (m, 2H), 1.37−1.22 (b, 20H).

*17-Hydroxyheptadecanenitrile (**4**).* Three grams (9.4 mmol) of the bromide **3** was dissolved in 60 mL of DMSO. Sodium cyanide (504 mg, 10.3 mmol) was added, and the mixture was stirred at 70 °C for 1 h. The mixture was cooled to room temperature and added to a separatory funnel containing 300 mL of water and 225 mL of ether. The water layer was separated and extracted three times with ether. The combined ether phases were washed once with 75 mL of brine, dried with $MgSO_4$ and filtered through a $MgSO_4$ plug, and the ether was evaporated. Yield: 1.93 g, yellowish solid (77%).

*Thioacetic Acid R,S-(16-Cyanohexadecyl) Ester (**5**).* Triphenylphosphine (2.748 g, 10.5 mmol) was dissolved in 28 mL of dry THF in a 250 mL round-bottom flask. The solution was cooled to 0 °C. Diisopropyl azodicarboxylate (2.118 g, 10.5 mmol) was added, and the solution was stirred for 40 min when a solution of 1.4 g of nitrile **4** (5.25 mmol) with 0.8 g of thiolacetic acid (5.25 mmol) in 28 mL of THF was slowly added through a transfer needle.

The temperature was kept at 0 °C for 1 h, and the solution was stirred for another 24 h at room temperature. The THF was rotovaped, and 10 mL of 15% ethyl acetate/85% hexane was added to the residue. The solution was filtered, and the filtrate was separated with column chromatography. The thioacetate **5** came second after a yellow impurity and before the triphenylphosphine oxide. The crude product (main impurity was triphenyl phosphine oxide) was recrystallized in methanol. Yield: 669 mg recrystallized product (39.4%). ^{1}H NMR ($CDCl_3$): δ 2.86 (t, 2H, J = 7.3 Hz), 2.34 (t, 2H, J = 7.1 Hz), 2.32 (s, 3H), 1.66 (m, 2H), 1.56 (m, 2H), 1.44 (m, 2H), 1.38−1.22 (b, 22H).

*17-Mercaptoheptadecanenitrile (**1**).* Thioacetate **5** (300 mg) was added to 40 mL of outgassed ethanol. The solution was warmed until it was clear, and 8 mL of 5 N NaOH was added with a syringe. The solution was stirred for 2 h at room temperature. Sixteen milliliters of 5 N HCl, 100 mL of freshly distilled ether, and 100 mL of water were added successively, and the ether phase was separated, dried with $MgSO_4$, and filtered through a $MgSO_4$ plug. NMR shows the methylene group next to the nitrile group at 2.34 ppm, complete hydrolysis (no more thioacetate CH_3 group at 2.32 ppm). The product was 90% thiol (multiplet at 2.52 ppm) and 10% disulfide (triplet at 2.68 ppm). ^{1}H NMR ($CDCl_3$): δ 2.52 (m, 2H), 2.34 (t, 2H, J = 7.2 Hz), 1.69−1.54 (m, 4H), 1.48−1.20 (b, 24H), 1.33 (t, 1H, J = 7.7 Hz).

2.2. Monolayer Preparation. The gold and silver substrates for the XPS and NEXAFS experiments were prepared by thermal evaporation of 200 nm of gold or 100 nm of silver (99.99% purity) onto polished 3 in. single-crystal silicon (100) wafers (Silicon Sense) that had been precoated with a 5 nm titanium adhesion layer. The coated wafers were cut with a diamond tip into 1 cm^2 sample pieces. The substrates for the wetting experiments were 2 in. silicon (100) wafers with thermally evaporated 5 nm chromium and 200 nm gold or silver films. Such evaporated films are standard substrates for thiol-derived SAMs. They are polycrystalline with a grain size of 20−50 nm as observed by atomic force microscopy. The grains predominantly exhibit a (111) orientation, which is, in particular, supported by the observation of the corresponding forward-scattering maxima in the angular distributions of the Au 4f photoelectrons[23] and by the characteristic binding energy (BE) shift of the Au 4f surface component.[24] The SAMs were formed by immersion of freshly prepared substrates into a 1 mM NC-C16 solution in absolute ethanol at room temperature for 24 h. After immersion, the samples were carefully rinsed with pure ethanol and blown dry with argon. No evidence for impurities or oxidative degradation products was found.

2.3. XPS and NEXAFS Spectroscopy. The NC-C16 SAMs were characterized by XPS and NEXAFS spectroscopy using a modified multitechnique ultrahigh vacuum (UHV) chamber[25] attached to the HE-TGM 2 beamline[26] at the German synchrotron radiation facility BESSY I in Berlin. The experiments were

performed at room temperature under UHV conditions (base pressure better than 1.5×10^{-9} Torr). The time for the NEXAFS/XPS characterization was selected as a compromise between the spectra quality and the damage induced by X-rays.[17,27−29]

The XPS measurements were performed with a Mg Kα X-ray source and a VG CLAM 2 spectrometer in normal emission geometry with an energy resolution of ∼0.9 eV. The X-ray source was operated at 260 W power and positioned ∼1 cm away from the samples. The energy scale was referenced to the Au $4f_{7/2}$ peak at 84.0 eV,[30] which resulted in a binding energy (BE) of 368.15 eV for the Ag $3d_{5/2}$ peak in agreement with handbook values of 368.3 eV[30] and 367.9 eV.[31] For each sample, a wide scan spectrum and the C 1s, O 1s, S 2p, and Au 4f or Ag 3d narrow scan spectra were measured. The narrow scan spectra were normalized to the integral intensity of the wide scan spectra to correct for small differences in sample positions and X-ray source intensities[6] and fitted by using a Shirley-type background[32] and symmetric Voigt functions[33] with a Gauss/Lorenz ratio of 4:1. To fit the S $2p_{3/2,1/2}$ doublet, we used a pair of such peaks with the same full width at half-maximum (fwhm), the standard[30] spin−orbit splitting of ∼1.2 eV (verified by fit), and the branching ratio of 2 ($S2p_{3/2}$/$S2p_{1/2}$). The fits were performed self-consistently: the same peak parameters were used for identical spectral regions.

The NEXAFS measurements were carried out at the C 1s and N 1s absorption edges in the partial electron yield mode with a retarding voltage of −150 and −350 V, respectively. Linear polarized synchrotron light with a polarization factor of ∼92% was used. The energy resolution was ∼0.65 eV. The incidence angle of the synchrotron light was varied from 90° (**E**-vector in surface plane) to 20° (**E**-vector near surface normal) in steps of 10°−20° to monitor the orientational order within the films. This approach is based on so-called linear dichroism in X-ray absorption, that is, the strong dependence of the cross section of the resonant photoexcitation process on the orientation of the electric field vector of the linearly polarized light with respect to the molecular orbital of interest.[34]

The raw NEXAFS spectra were normalized to the incident photon flux by division through a spectrum of a clean, freshly sputtered gold sample. In the case of NC-C16/Ag, a spectrum of clean silver was subtracted from the raw spectrum of a SAM sample before the normalization.[6,35] The energy scale was referenced to the pronounced π_1* resonance of highly oriented pyrolytic graphite at 285.35 eV.[36]

2.4. Wetting Properties. The uncut 2 in. wafer samples were put on a Ramé−Hart contact angle goniometer equipped with a motor to move the sample stage horizontally under the droplet. The latter was attached to a needle at the end of a syringe filled with ultrapure water (Millipore system, 18 MΩ cm). Ten microliter water droplets were put on the surface, and images of the drop silhouette were taken with a video camera and stored for analysis on a computer while the stage was moved at a speed of 0.05 mm per second.

3. Results

3.1. XPS Measurements. XPS spectra provide quantitative information on the composition, chemical identity, and effective thickness of the investigated films. The C 1s, N 1s, and S 2p spectra of the NC-C16 SAMs on Au and Ag are presented in Figure 1. The vertical scale is the same for the spectra in identical spectral regions. The higher background intensity and lower signal-to-noise ratio of the S 2p and C 1s spectra for NC-C16/Au as compared to NC-C16/Ag are related to inelastic electrons originated from the Au 4f photoelectrons (BE below the S 2p and C 1s ionization thresholds). The relatively poor signal-to-noise ratio of the S 2p spectra is explained by the attenuation of the corresponding signal by the overlayer and a relatively short acquisition time chosen to reduce possible X-ray-induced damage during the measurements.[17,27−29] The comparatively poor signal-to-noise ratio of the N 1s spectra stems from a large inelastic background.

In the C 1s spectra in Figure 1a,b, a pronounced C 1s photoemission maximum with a higher BE shoulder is observed. The BE positions of the main maxima (284.95 eV for NC-C16/Au and 285.15 eV for NC-C16/Ag) are very close to the respective values for nonsubstituted (CH_3-terminated) AT SAMs on Au and Ag (284.85 and 285.25 eV, respectively).[24,35] Whereas the main C 1s emission can be unequivocally attributed to the carbon atoms in the aliphatic matrix, the shoulder at a higher BE can only be related to the occurrence of the −CN group: such a shoulder is not observed in the XPS spectra of nonsubstituted ATs. Exclusively assigning the shoulder to the nitrile carbon, we fitted it by a single peak and got a ratio between the intensities of the main and nitrile-related peaks of 4.5−5. After a correction for the attenuation of the C 1s signal, this intensity ratio gave us a nonrealistic value of ∼8.1 for the ratio between the numbers of the nitrile and methylene groups. At the same time, a fit of the shoulder by two peaks[10] results in stoichiometric intensity ratio of ∼16 after the attenuation correction. These two peaks can only be assigned to the carbon atoms in the nitrile functionality and nitrile-adjacent methylene group, which means that the BE of the carbon atom in the latter group experiences a chemical shift (∼1.3 eV) due to the bonding to the nitrile group. The nitrile carbon exhibits a larger chemical shift of ∼2.2 eV with respect to the carbon atoms in the alkyl matrix.

In the N 1s spectra in Figure 1c,d, a single emission related to the nitrile nitrogen is observed. The BEs of this emission for Au and Ag are very close to each other: 399.95 eV for NC-C16/Au and 400.0 eV for NC-C16/Ag.

In the S 2p spectra in Figure 1e,f, a single S $2p_{3/2}$/S $2p_{1/2}$ doublet is observed for both NC-C16/Au and NC-C16/Ag. This doublet is usually associated with a thiolate species bonded to the metal surface and is typical for the intact thiol-derived SAMs.[10,12,35,37,38] Similar to nonsubstituted AT SAMs,[24,35] the BEs of this doublet for Au and Ag are very close to each other: 162.1 eV for NC-C16/Au and 161.85 eV for NC-C16/Ag.

The integral intensities of the C 1s, N 1s, and S 2p emissions for NC-C16/Ag are larger by 15−35% than those for NC-C16/Au, which implies a higher packing density and a smaller inclination of the alkyl chains on Ag. The same conclusion results from the analysis of the Au 4f and Ag 3d spectra (not shown) for NC-C16/Au and NC-C16/Ag, respectively. Considering the attenuation of the Au 4f and Ag 3d photoelectrons by the hydrocarbon overlayer, we got an effective thickness of 19.7 and 23.5 Å for NC-C16/Au and NC-C16/Ag, respectively. Note that the attenuation lengths of the Au 4f and Ag 3d photoelectrons were taken as 31 and 26 Å, respectively (Mg Kα X-ray source).[5,39] Note also that the comparison of the derived effective thicknesses to the analogous values for nonsubstituted AT SAMs on Au and HO-substituted AT films on Ag suggested lower packing densities of NC-C16/Au and NC-C16/Ag.

3.2. NEXAFS Measurements. NEXAFS experiments provide both chemical and structural information about the occurrence and average orientation of unoccupied molecular orbitals within organic films of interest. The C 1s NEXAFS spectra of NC-C16/Au and NC-C16/Ag are depicted in Figure 2, panels a

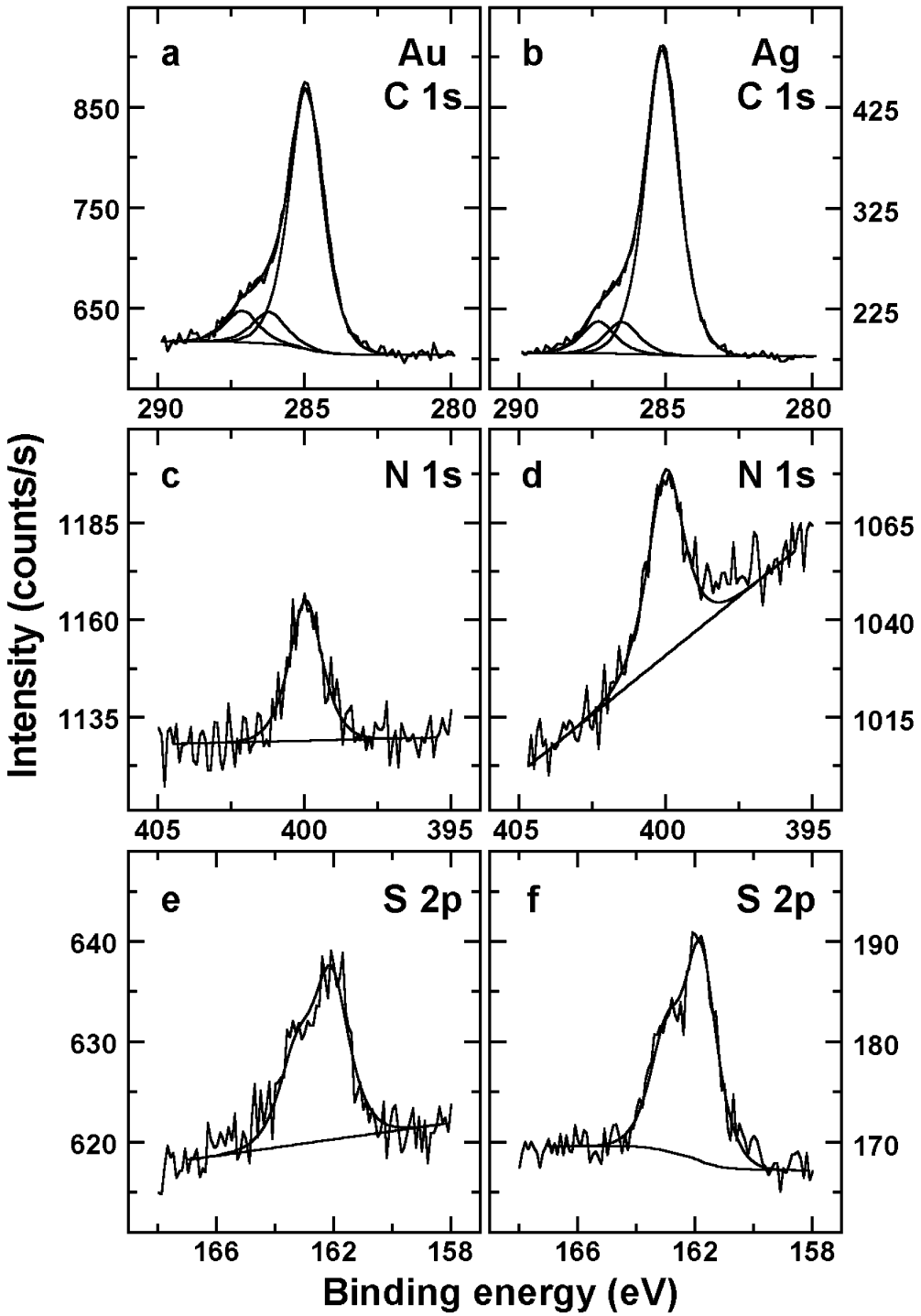

Figure 1. The C 1s (a, b), N 1s (c, d), and S 2p (e, f) XPS spectra collected from the NC-C16 films on Au (a, c, and e) and Ag (b, d, and f) substrates. The C 1s emission structures are fitted by three Voigt functions (solid lines). Only one Voigt function was used to fit the N 1s spectra. The S $2p_{3/2}$/S $2p_{1/2}$ doublet was decomposed using two Voigt functions with the same fwhm and Gauss/Lorentz proportion. See text for details.

and b, respectively. The corresponding N 1s spectra are presented in Figure 3a,b.

All spectra in Figure 2 exhibit a C 1s absorption edge related to C 1s → continuum excitations, several pronounced π^* and σ^* resonances, and two overlapping R* resonances (excitations into orbitals of dominantly Rydberg character).[40−42] The assignments of these resonances are given in Table 1; they were performed in accordance with refs 34, 40, and 43−47. The intensities of the resonances vary strongly when the angle of incidence of the X-rays is changed, which is additionally emphasized by the difference spectra (bottom curves). The pronounced linear dichroism suggests a relatively high orientational order for both NC-C16/Au and NC-C16/Ag, while the signs of the resonance-related peaks in the difference spectra imply an upright orientation of the alkyl chains. Also, a distinct π^*(C≡N*) resonance in the N 1s NEXAFS spectra of these films exhibits a clear linear dichroism, which suggests that the −CN moieties have a predominant orientation. The photon energy (PE) position of this resonance is 400.83 and 400.82 eV for NC-C16/Au and NC-C16/Ag, respectively. These values are somewhat lower than the theoretical estimate for long-chain *n*-alkylnitriles (401.87 eV)[48] but slightly exceed the respective experimental PEs for HCN[49] and CH_3CN.[50] Considering the errors of the theoretical calculations[48] and an increase in the

TABLE 1: Positions and Assignments of the C 1s NEXAFS Resonances for NC-C16/Au and NC-C16/Ag

spectral feature	photon energy for NC-C16/Au (eV)	photon energy for NC-C16/Ag (eV)	fwhm (eV)	assignment	reference photon energy (eV)
step 1	287.8	287.8	1.7	$-C^*H_2-$	287.8 [44]
step 2	289.6	289.6	1.7	$C^*N-C^*H_2-$	from XPS
peak 1	285.3	285.3	1.2−3.05	contamination, excitation into alkane−metal orbitals	285.5 [46] 285.1 [47]
peak 2	286.8	286.9	0.6	π^*(C−N)	286.4 [34]
peak 3	287.4	287.5	0.6	R_σ^*	287.4 [40]
peak 4	288.0	288.1	0.6	R_π^*	288.1 [40]
peak 5	289.4	289.4	1.1	σ-like or C*−S	
peak 6	292.8	293.2	3.4	σ^*(C−C)	293.4 [44]
peak 7	300.0	300.0	11.5−12.0	σ^*(C−C′)	301.6 [44]

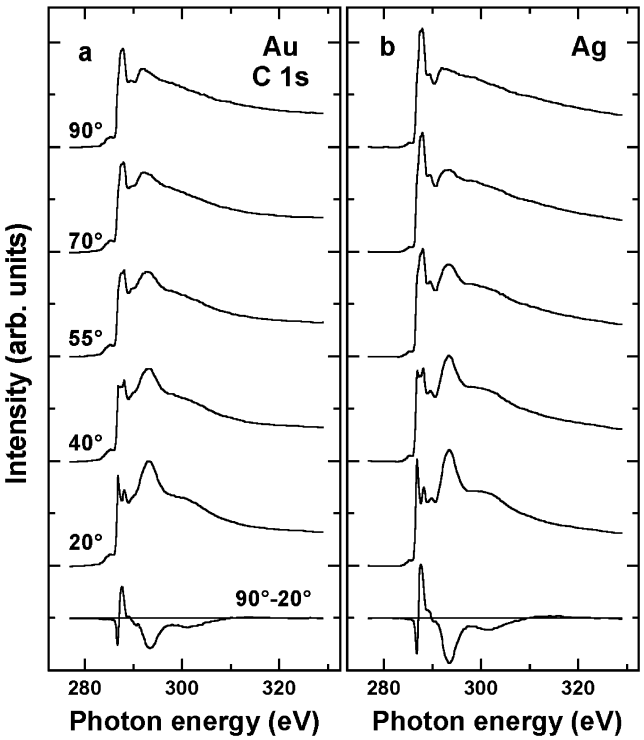

Figure 2. The C 1s NEXAFS spectra collected from NC-C16/Au (a) and NC-C16/Ag (b). The bottom curves in panels a and b represent the difference of the spectra acquired at incidence angles of 90° and 20°.

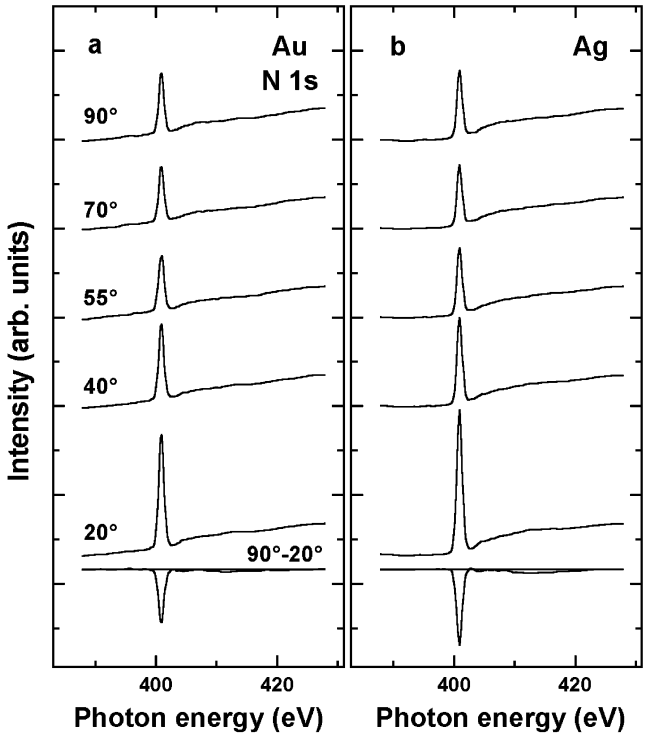

Figure 3. The N 1s NEXAFS spectra collected from NC-C16/Au (a) and NC-C16/Ag (b). The bottom curves in panels a and b represent the difference of the spectra acquired at incidence angles of 90° and 20°.

PE for the π^*(C≡N*) resonance with increasing length of the aliphatic chain,[48] the obtained PE positions of this resonance in NC-C16/Au and NC-C16/Ag agree well with the previous results.

Except for the qualitative conclusion on the orientational order in the NC-C16 SAMs, values of the average tilt angle of the alkyl chains and −CN functionalities in these films can be obtained by a quantitative analysis of the angular dependence of the NEXAFS resonance intensities.[34] Whereas the respective intensities can be derived directly from the N 1s spectra, a decomposition of the C 1s spectra is necessary. This decomposition was performed self-consistently for the entire spectra series; several Gauss-like peaks and two adsorption edges were used to fit the spectra following the recipes of ref 34. The second, low-intensity absorption edge was introduced to represent the carbon atoms in the nitrile group and the nitrile-adjacent methylene moiety. This edge was shifted upward by ∼1.8 eV (an average of 1.3 and 2.2 eV) with respect to the major edge following the difference between the BE positions of the respective maxima in the C 1s XPS spectra in Figure 1a,b. A typical fit of C 1s NEXAFS spectra of NC-C16/Au and NC-C16/Ag is depicted in Figure 4; the 55° spectra are taken as an example.

The derived intensities of the most pronounced π^*(C*≡N), σ^*(C−C), and R* resonances are presented in Figure 5 as functions of the incidence angle of the X-rays, along with the intensities of the π^*(C≡N*) resonance taken from the N 1s NEXAFS spectra. For comparison, the theoretical dependencies for different tilt angles of the alkyl chains and −CN moiety are added as thin solid lines. These dependences were calculated on the basis of the standard expressions describing angular dependence of the transition matrix elements for the cases of so-called "vector" and "plane" orbitals.[34] The π^*(C*≡N) and R* ($R_\sigma^* + R_\pi^*$) orbitals were considered as plane orbitals, while the σ^*(C−C) was regarded as a vector orbital following the assignments of ref 45. Accordingly, γ is the angle between the sample normal and the normal to the π^*(C≡N) or R* plane, while φ is the angle between the sample normal and the vector along the σ^*(C−C) orbital. The derived values of γ and φ are indicated at the respective data.

Because the R* orbital is perpendicular to the alkyl chain axis and the σ^*(C−C) orbital is directed along this axis,[40,44,45]

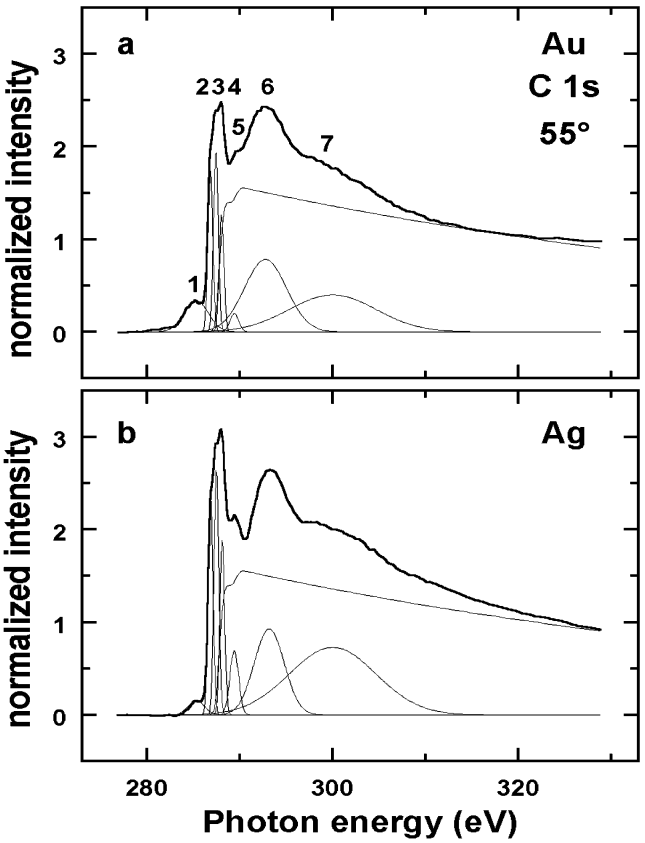

Figure 4. A fit of the C 1s NEXAFS spectra of NC-C16/Au (a) and NC-C16/Ag (b). The 55° spectra are taken as an example. The entire spectra sets in Figure 2a,b were fitted self-consistently.

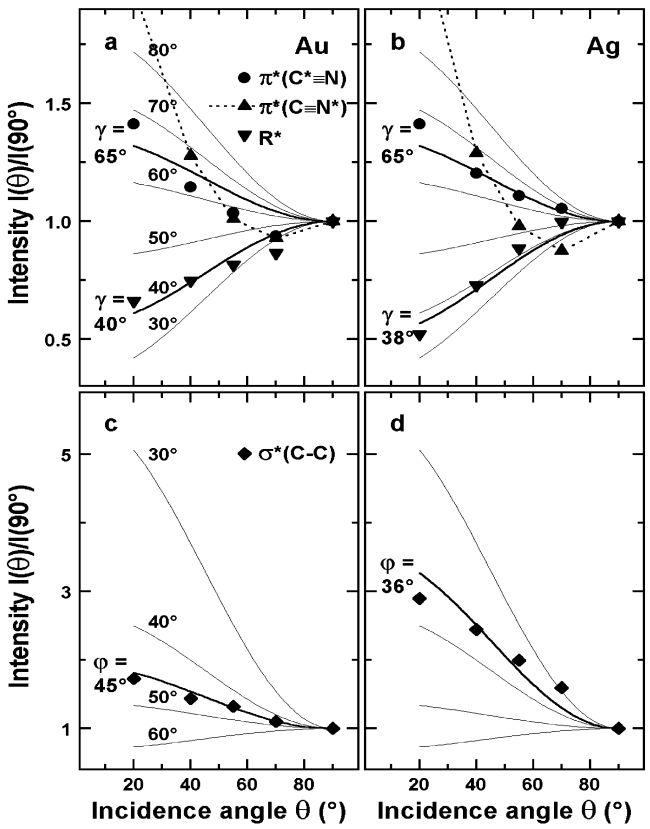

Figure 5. The intensity of the π^*(C*≡N) (a, b), σ^*(C−C) (c, d), R* (a, b), and π^*(C≡N*) (a, b) resonances for NC-C16/Au (a, c) and NC-C16/Ag (b, d) as a function of the incidence angle of the X-rays. For comparison, the theoretical dependencies for different tilt angles of the alkyl chains and C≡N moiety are added as thin solid lines. The π^*-(C≡N) and R* orbitals were considered as plane orbitals, while the σ^*(C−C) was regarded as a vector orbital. Accordingly, γ is the angle between the sample normal and the normal to the π^*(C≡N) or R* plane, while φ is the angle between the sample normal and the vector along the σ^*(C−C) orbital. The derived values of γ and φ are indicated at the respective data. Note that the superposition of the R_σ* and R_π* orbitals can be considered as a plane orbital because both vector constituents are perpendicular to each other and have similar oscillator strengths.[34,40]

both γ and φ are average tilt angles of the alkyl chains. The derived values of γ are 40° (Au) and 38° (Ag) for the R* orbital, while the values of φ are 45° (Au) and 36° (Ag) for the σ^*-(C−C) orbital. Taking the mean of these values, we got an average tilt angle of the alkyl chain of 42.5° and 37° for NC-C16/Au and NC-C16/Ag, respectively.

As to the −CN moiety, the angle γ describes the orientation of the C≡N axis with respect to the sample normal. Considering the data for π^*(C≡N*) resonance, one sees that the respective dependences do not follow the theoretical curves, which makes impossible the estimate of γ. We believe that this problem is related to the difficulties in the normalization of the N 1s NEXAFS spectra (Figure 3), which do not reveal a pronounced absorption edge. At the same time, the data for the π^*(C*≡N) resonance can be roughly described by the theoretical dependences, especially in the case of NC-C16/Ag. The derived value of γ is ∼65° for both NC-C16/Au and NC-C16/Ag.

It should be mentioned that the fits presented in Figure 4 are the result of the optimization of all relevant parameters. In doing such an optimization, a large importance has a position and a width of the major absorption edge, which have to be preset before the fitting procedure. Even though these parameters are optimized in the course of the fitting procedure and the resulting values agree well with literature data,[16,44] the initial settings influence the results. To avoid this ambiguity and to perform an independent proof of the derived tilt angles, we processed the C 1s NEXAFS data using the difference spectra, which are presented in Figure 6. As described in refs 34, 43, and 51, upon subtracting two NEXAFS spectra recorded at different X-ray incidence angles θ and θ_1, one gets for a plane orbital

$$I_p(\theta) - I_p(\theta_1) = C(1 - \cos^2\gamma)(\cos^2\theta - \cos^2\theta_1) \quad (1)$$

where $I_p(\theta)$ and $I_p(\theta_1)$ are the resonance intensities and C is a normalization constant that depends on the excitation probability from the C 1s core level into a given molecular orbital. Even though the latter parameter is unknown, the expression 1 can be used for the evaluation of the NEXAFS spectra, if one has a reference sample with the same molecular orbitals and a known molecular structure.

As such reference samples, we used SAMs formed from $CH_3(CH_2)_{15}SH$ (C16), $CH_3(CH_2)_{17}SH$ (C18), and $HO(CH_2)_{16}$-SH (HO-C16) on Au and films fabricated from HO-C16 on Ag. In accordance with previous NEXAFS investigations,[16,44] we assumed that the average tilt angles of the alkyl chains in these systems are equal to 35° for C16/Au, C18/Au, and HO-C16/Au. Considering that no significant changes in the orientation of the alkyl chains in nonsubstituted AT SAMs on Au occur upon replacing the terminal $-CH_3$ group by the −OH moiety,[16] we assumed that the average tilt angle of the alkyl chains in HO-C16/Ag does not differ significantly from that in the nonsubstituted AT SAMs on Ag[12,35,38,52] and is approximately equal to 12°.

We used R* and π^*(C*≡N) resonances to derive qualitative and quantitative information on the orientation of the alkyl chains and −CN moiety in the NC-C16 SAMs. The intensities

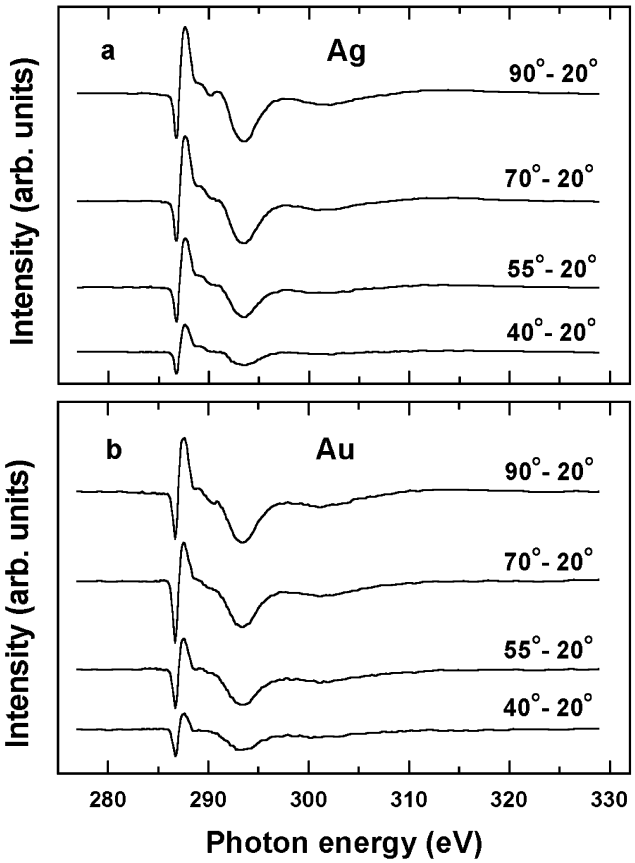

Figure 6. The differences of the NEXAFS spectra recorded at X-ray incidence angles 40°−90° and 20° for NC-C16/Au (a) and NC-C16/Ag (b).

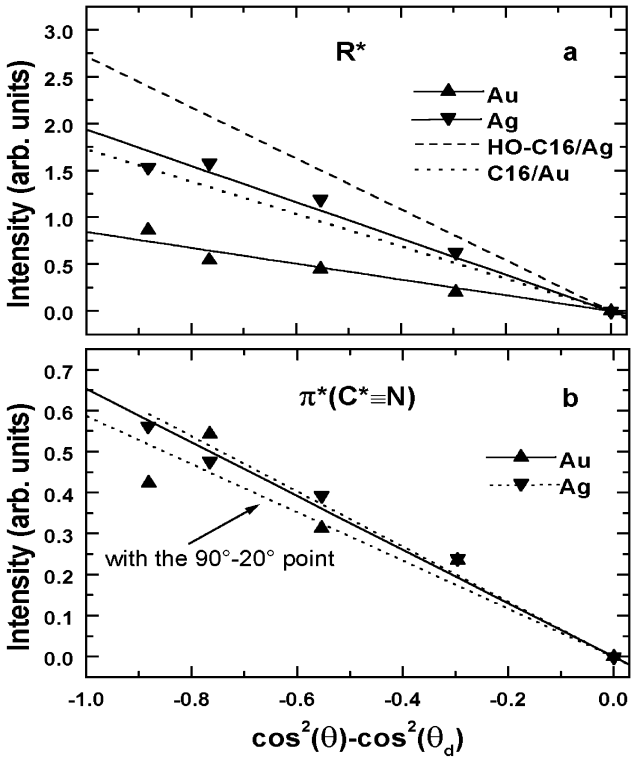

Figure 7. Plots of the intensities of the R* (a) and π^*(C*≡N) (b) difference peaks (see Figure 6) for NC-C16/Au (▲) and NC-C16/Ag (▼) versus $\cos^2\theta - \cos^2\theta_d$ ($\theta_d = 20°$) with the respective linear fits (the solid lines) using least-squares analysis. The analogous fits for the reference samples, C16/Au (the dotted line) and HO-C16/Ag (the dashed line) are presented in panel a for comparison. A fit for NC-C16/Au (dashed line) in panel b was performed both with and without the consideration of the data point derived from the "90°−20°" spectrum.

of the respective difference peaks were derived by numerical integration of the difference spectra (Figure 6) in the energy intervals 286.1−287.0 and 287.0−288.6 eV for the π^*(C*≡N) and R* resonances, respectively. The plots of the intensities of the R* and π^*(C*≡N) difference peaks for NC-C16/Au and NC-C16/Ag versus $\cos^2\theta - \cos^2 20°$ are depicted in Figure 7, along with the lines that are best fits to the data using least-squares analysis based on eq 1. The analogous fits for two reference samples, C16/Au (dotted line) and HO-C16/Ag (dashed line), are presented in Figure 7a for comparison. It is clearly seen that the slopes of the linear fits for NC-C16/Au and NC-C16/Ag are noticeably smaller than the slopes of the lines for the respective reference samples: C16/Au for NC-C16/Au and HO-C16/Ag for NC-C16/Ag, which means a larger tilt of the alkyl chain in the case of the −CN substitution. Quantitative evaluation based on the C16/Au, C18/Au, and HO-C16/Au standards gives values of 44°, 44°, and 41°, respectively, for the average tilt angle of alkyl chains in NC-C16/Au. For NC-C16/Ag, the same procedure results in average tilt angles of 30° and 29° using the C16/Au and HO-C16/Ag reference samples, respectively. Thus, the values derived on the basis of different standards are very close to each other, which emphasizes their reliability. In addition, the values for NC-C16/Au practically coincide with the average tilt angle derived via the fitting of the resonance intensities. Only in the case of NC-C16/Ag, there is a difference of ∼7° between the average tilt angles obtained from the spectra difference approach (29°, 30°) and from the fitting of the resonance intensities (37°).

In the case of the π^*(C*≡N) resonance, a quantitative evaluation of the data presented in Figure 7b is not possible because of the absence of a suitable reference sample containing the −CN functionality in a known orientation. Therefore, only a conclusion on relative orientation of these functionalities in NC-C16/Au and NC-C16/Ag can be made. Considering the data presented in Figure 7b, one finds that the linear fits for NC-C16/Au and NC-C16/Ag have almost the same slopes, as soon as the data point derived from the "90°−20°" spectrum for NC-C16/Au is not taken into account. The inclusion of this point will result in only a minor increase in the slope of the respective linear fit, which means only a slight increase in the tilt angle of the −CN functionality. Thus, average tilt angle of the −CN functionality in HO-C16/Au is very close to or slightly exceeds that for NC-C16/Ag, which agrees well with the results of the direct fitting (∼65° for both NC-C16/Au and NC-C16/Ag).

3.3. Water Contact Angle Measurements. NC-C16/Au showed advancing (θ_a) and receding contact angles (θ_r) of 75° and 54°, respectively (see Figure 8). On Ag, both angles are slightly sharper with $\theta_a = 69°$ and $\theta_r = 52°$. The hysteresis $\theta_a - \theta_r$ is relatively large in comparison with the previously[53] reported <10° differences for similarly wettable methyl ester surfaces, especially if we consider that ($\cos\theta_a - \cos\theta_r$) is the real thermodynamic measure for the difference between the surfaces immediately before and after wetting. The larger hysteresis of the nitrile-terminated surfaces indicates that the small −CN end group has some space for rearrangements. The nitrile end groups are buried inside the nonwetted film and rearrange and become more exposed as soon as the droplet contacts the film surface.

The average $(\theta_a + \theta_r)/2$ contact angle is 64.5° on Au and 60.5° on Ag. That is far less hydrophobic than methyl- or methylene-terminated surfaces (100°−115°) and even below the 85°−78° for methoxy-terminated monolayers. The dipole mo-

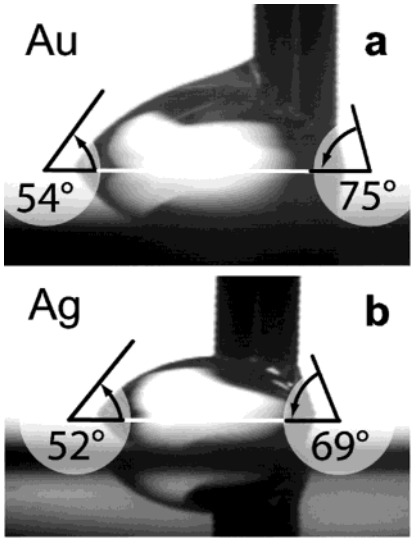

Figure 8. Dynamic advancing and receding water contact angles of NC-C16/Au (a) and NC-C16/Ag (b). The tip with the attached water droplet was kept still while a motor moved the underlying sample stage horizontally with a constant speed of 0.05 mm per second.

ment of the −CN group and the free electron pair at the nitrogen atom produce a surface that is as hydrophilic as a surface with densely packed methyl ester groups[53] or oligo(ethylene glycol)[4] derivatives such as $-(OCH_2CH_2)-OCH_3$. The nitrile group is the only two-atom end group so far that both is hydrophilic and fulfills all four molecular characteristics[18] that usually correlate with low protein adsorption (large polarity, a hydrogen bond accepting group, no hydrogen bond donating groups, and no net charge).

4. Discussion

The XPS, NEXAFS, and contact angle data imply that NC-C16 forms ordered, densely packed SAMs on polycrystalline gold and silver substrates with predominantly (111) orientation. The NC-C16 molecules are bonded to the substrate in the same manner as those in nonsubstituted AT SAMs, as concluded from the observation of the characteristic S 2p doublet in the XPS spectra.

The XPS data suggest a higher packing density or a larger effective thickness for NC-C16/Ag as compared to NC-C16/Au. The latter parameter was estimated to be 23.5 and 19.7 Å for NC-C16/Ag and NC-C16/Au, respectively. A chemical shift of ∼2.2 eV for nitrile carbon and ∼1.3 eV for the carbon atom in the nitrile-adjacent methylene group were found in good agreement with previous results.[10]

The C 1s and N 1s NEXAFS spectra reveal absorption resonances that are characteristic for the intact NC-C16 SAMs. A pronounced linear dichroism of these resonances suggests a good orientational order in the NC-C16 films. The signs of the resonance peaks in the difference NEXAFS spectra implies an upright orientation of the alkyl chains and a predominant orientation of the −CN moieties within the surface plane for both NC-C16/Au and NC-C16/Ag. A quantitative evaluation of the NEXAFS data was performed in two different ways—via the fitting of the resonance intensities and via the difference spectra approach.

The resonance intensities derived from the N 1s NEXAFS spectra behave in a similar way for NC-C16/Au and NC-C16/Ag but do not follow a theoretical expression for the resonance intensity vs the incidence angle of the X-rays, which is presumably related to the difficulties in the normalization of the N 1s NEXAFS spectra. Because of the same reason, the difference spectra approach does not work for the N 1s data as well.

In the case of the C 1s NEXAFS spectra, both fitting of the resonance intensities and the difference spectra approach lead to reasonable results. The former procedure gives values of 42.5° and 37° for the average tilt angle of the alkyl chains in NC-C16/Au and NC-C16/Ag, respectively, and a value of 65° for the average tilt angle of the −CN moieties in both of these systems. The derived tilt angles vary somewhat depending on the preset of the absorption edges within the spectra fitting procedure. The difference spectra approach results in values of 41°−44° and 29°−30° for the average tilt angle of the alkyl chains in NC-C16/Au and NC-C16/Ag, respectively. For the −CN moiety, only a qualitative estimate was possible. The data suggest a similar orientation of the −CN moieties in NC-C16/Au and NC-C16/Ag with a slightly larger tilt of these moieties in NC-C16/Au than in NC-C16/Ag.

The contact angle measurements indicate that the SAM/ambient interface consists, as expected, of the terminal −CN groups. The large hysteresis of the contact angle implies that these groups have some space for rearrangements, which agrees with their orientation derived from the NEXAFS data. The in-surface-oriented nitrile groups can easily rearrange and become more exposed as soon as the droplet contacts the film surface.

Considering all experimental data together, we can conclude that the results of the different experimental techniques and different data processing approaches agree quite well. A larger packing density, a smaller inclination of the alkyl chains, and a higher degree of the orientational and conformational order is observed for NC-C16/Ag as compared to NC-C16/Au (the latter conclusion is also supported by the preliminary infrared reflection spectroscopy (IRS) results).[54] Also, similar orientations of the −CN functionalities, predominantly in the surface plane, occur in both systems. The average tilt angle of the alkyl chains in NC-C16/Au was estimated to be 42.5°. In the case of NC-C16/Ag, we have to choose between the somewhat different values obtained from the difference spectra approach (29.5°) and from the fitting of the NEXAFS resonance intensities (37°). Taking into account the noticeable difference in the XPS-derived effective thicknesses for NC-C16/Au and NC-C16/Ag, the above-mentioned ambiguity of the spectra fitting, and preliminary results of infrared spectroscopy experiments,[55] we rather trust the results of the difference spectra approach, which infers that an average tilt angle of the alkyl chains in NC-C16/Ag is equal to 29.5°. The average tilt angle of the −CN moieties in NC-C16/Au and NC-C16/Ag was found to be 65°.[56] The error of the derived angles is estimated to be ±5° and ±7° for the tilt angles of the alkyl chains and −CN moieties, respectively. A value of ±5° is a standard accuracy for the NEXAFS-derived tilt angles, whereas the second value (±7°) takes into account large deviations of the respective experimental data from the theoretical curves (Figure 5). Note that the obtained tilt angles for the −CN moieties agree quite well with the theoretical estimate from ref 13. The latter value is equal to 71.5°. It could be derived on the basis of the calculated values for out-of-plane and in-plane components of the average dipole moment of the −CN functionality in NC-C16/Au.[13]

These results have to be compared with the analogous parameters for the nonsubstituted AT SAMs on Au and Ag. In this context, it is worth mentioning that even for these "simple" systems the measured tilt angles depend on the technique applied:[39] slightly different values are derived from IR specroscopy,[12] X-ray diffraction,[4,57,58] and NEXAFS[43−46] data. The

difference is presumably related to the intrinsic features of the above-mentioned methods. In particular, X-ray-diffraction probes only the ordered (crystalline) regions,[4] whereas NEXAFS spectroscopy gives an average value of the tilt angle over the X-ray spot region, including both ordered and disordered (domain boundaries, defect sites, etc.) areas. This is probably the reason that the latter tilt angles exceed the values derived from X-ray diffraction by several degrees. Keeping this difference in mind, we still prefer to use the tilt angles determined by the same method as that used in the present study (NEXAFS spectroscopy) for the comparison.

The NEXAFS-derived (average) tilt angles of the alkyl chains in the nonsubstituted AT SAMs on Au and Ag are ~35° and ~12°, respectively.[35,38,43−46] It is then obvious that the substitution of weakly interacting $-CH_3$ tailgroups by strongly interacting polar groups results in a noticeable disordering or reorientation or both of the AT SAMs on both Au and Ag. The disordering presumably occurs through the formation of gauche defects in the alkyl chains, which have a zigzag planar conformation in nonsubstituted, long-chain AT SAMs. For NC-C16/Au, the degree of this disordering is comparable with that for AT SAMs with −COOH tailgroup,[16] in which the average tilt angle of the alkyl chains is larger by 7.5°−8° than this value in nonsubstituted AT/Au. The reason for the disordering in the carboxylic-acid-substituted SAMs is presumably strong hydrogen bonds between the −COOH groups, which lead to their dimerization and subsequently prohibit the formation of well-ordered films. In the case of the −CN groups, it is a strong electrostatic interaction between these moieties that distorts the orientational order. Theoretical estimates showed that such an interaction can even result in the formation of an ordered, ferroelectric structure at the SAM−ambience interface.[13] The respective 2D lattice formed by the polar −CN groups should be rotated and distorted with respect to the underlying arrangement formed by AT chains.[13] The formation of this hypothetical ordered lattice cannot of course be proven by either XPS or NEXAFS spectroscopy but rather by surface-sensitive scattering experiments such as He beam diffraction (e.g., see ref 59).

What can, however, be done, it is to consider the orientation of the −CN groups in the NC-C16 SAMs and compare it with the expected orientation in the case of all-trans conformation and the standard[12] tilt and twist of the AT chains. Assuming the substrate−S−C bonding angles around 104° for AT/Au and 180° for AT/Ag,[7,8,12,52] one gets "theoretical" tilt angles of the −CN moiety of 59.3° and 25.7° for NC-C16/Au and NC-C16/Ag, respectively. Another reference is the set of experimental values for the tilt angle of the methyl entity in the AT SAMs with an even number of methylene units in the alkyl chain. These angles were estimated to equal 53°[52] and 58°[60] for AT/Au and 27°[52] or 38.1°[60] for AT/Ag, close to the calculated values. Comparing these values with the derived average tilt angles of the −CN moieties in NC-C16/Au and NC-C16/Ag (65°), one finds that there is only a slight reorientation of the −CN moiety in NC-C16/Au due to the electrostatic interaction, whereas the reorientation of these groups in NC-C16/Ag is quite large (27°−39°). This higher extent of the reorientation agrees well with a large increase in the average tilt angle of alkyl chains in NC-C16/Ag as compared to the nonsubstituted AT SAMs on Ag. This increase can be related to both a disordering and a completely new arrangement of the AT chains in NC-C16/Ag as compared to the nonsubstituted SAMs. Taking into account the IR data for NC-C16/Ag, we rather believe that a rearrangement is the case.

5. Summary and Future Work

Chemical identity, packing density, and orientational and conformational order in SAMs formed from nitrile-functionalized alkanethiols on (111) gold and silver substrates were studied by using XPS, NEXAFS spectroscopy, and contact angle measurements. The NEXAFS spectra were acquired at the C 1s and N 1s absorption edges with both direct fitting and the difference spectra approach applied to process the data. The results of the different experimental techniques and different procedures of the data processing agree quite well with one another and suggest that NC-C16 form well-ordered, densely packed SAMs on (111) gold and silver substrates. A larger packing density, a smaller inclination of the alkyl chains, and a higher degree of the orientational and conformational order were found in NC-C16/Ag as compared to NC-C16/Au. The average tilt angles of these chains in NC-C16/Ag and NC-C16/Au were estimated to be 29.5° ± 5° and 42.5° ± 5°, respectively. The −CN functionalities were found to be predominantly oriented in the surface plane with same tilt angle of 65° ± 7° in both NC-C16/Au and NC-C16/Ag. This orientation is beneficial to minimize the electrostatic interaction between the −CN moieties but different from the standard orientation of the functional groups in nonsubstituted AT SAMs of the same chain length.

Comparison with the SAMs formed from the nonsubstituted ATs suggests that the strongly interacting nitrile entities have a strong influence on the molecular orientation, packing, and structure of AT films on both Au and Ag substrates. The substitution of the weakly interacting methyl groups by the nitrile entities results in increase in the average tilt angles of the alkyl chains by ~7.5° and ~17.5° in AT/Au and AT/Ag, respectively. This increase is presumably related to the disordering of the alkyl chains (via the formation of gauche defects) in NC-C16/Au and their rearrangement (as compared to the respective nonsubstituted AT SAM) in NC-C16/Ag due to a strong electrostatic interaction between the polar −CN moieties, which distorts the underlying 2D-lattice formed by AT chains. These types of effects are very important because they offer a means to control and understand the detailed structure of a SAM and its ambient surface for applications such as tailored wetting and biologically active surfaces. Accordingly, to better define the conformational order, molecular orientation, and translational order correlations in these SAMs, work is underway on the application of quantitative infrared reflection spectroscopy (IRS) and molecular resolution atomic force microscopy. The preliminary IRS results support both the conclusion about a significant decrease in chain conformational order and molecular orientation changes in NC-C16/Au compared to SAMs on Ag.[54] The combination of these results with the XPS and NEXAFS data will provide more accurate structural characterizations.

NEXAFS spectroscopy was found to be capable of providing information on the orientation of small tail groups in self-assembled monolayers, even though some problems related to a correct normalization of the absorption spectra have to be overcome in the future.

Another interesting issue is the orientation of the −CN functionalized AT SAMs with an odd number of methylene units in the alkyl chain. Preliminary experiments on SAMs formed from $NC(CH_2)_{15}SH$ (NC-C15) on Au exhibit noticeable differences as compared to NC-C16/Au, giving rise to so-called odd−even effects.[54] This work will be reported in future publications.

Acknowledgment. The authors are very grateful to M. Grunze for his support. We thank the BESSY staff, especially

M. Mast for technical help, K. Heister for assistance at BESSY, G. Albert for preparation of the substrates, and Ch. Wöll (Universität Bochum) for providing us with experimental equipment. This work has been supported by the German BMBF (Grants 05 SF8VHA 1 and GRE1HD), Deutsche Forschungsgemeinschaft (Grant JA 883/4-1), the Fonds der Chemischen Industrie, the U.S. Defense Advanced Research Program Agency and Office of Naval Research (Grant DARPA/ONR; for D.L.A. and P.H.), and the U.S. National Science Foundation (D.L.A.).

References and Notes

(1) Ulman, A. *An Introduction to Ultrathin Organic Films: Langmuir−Blodgett to Self-Assembly*; Academic Press: New York, 1991.
(2) Ulman, A. *Chem. Rev.* **1996**, *96*, 1533.
(3) *Thin films: self-assembled monolayers of thiols*; Ulman, A., Ed.; Academic Press: San Diego, CA, 1998.
(4) Schreiber, F. *Prog. Surf. Sci.* **2000**, *65*, 151.
(5) Harder, P.; Grunze, M.; Dahint, R.; Whitesides, G. M.; Laibinis, P. E. *J. Phys. Chem. B* **1998**, *102*, 426.
(6) Frey, S.; Heister, K.; Zharnikov, M.; Grunze, M.; Tamada, K.; Colorado, R., Jr.; Graupe, M.; Shmakova, O. E.; Lee, T. R. *Isr. J. Chem.* **2000**, *40*, 81.
(7) Zharnikov, M.; Frey, S.; Rong, H.; Yang, Y. J.; Heister, K.; Buck, M.; Grunze, M. *Phys. Chem. Chem. Phys.* **2000**, *2*, 3359.
(8) Rong, H. T.; Frey, S.; Yang, Y. J.; Zharnikov, M.; Buck, M.; Wühn, M.; Wöll, Ch.; Helmchen, G. *Langmuir* **2001**, *17*, 1582.
(9) Zharnikov, M.; Grunze, M. *J. Phys.: Condens. Matter.* **2001**, *13*, 11333.
(10) Bain, C. D.; Troughton, E. B.; Tao, Y.-T.; Evall, J.; Whitesides, G. M.; Nuzzo, R. G. *J. Am. Chem. Soc.* **1989**, *111*, 321.
(11) Nuzzo, R. G.; Dubois, L. H.; Allara, D. L. *J. Am. Chem. Soc.* **1990**, *112*, 558.
(12) Laibinis, P. E.; Whitesides, G. M.; Allara, D. L.; Tao, Y.-T.; Parikh, A. N.; Nuzzo, R. G. *J. Am. Chem. Soc.* **1991**, *113*, 7152.
(13) Hautman, J.; Bareman, J. P.; Mar, W.; Klein, M. L. *J. Chem. Soc., Faraday Trans.* **1991**, *87*, 2031.
(14) Laibinis, P. E.; Whitesides, G. M. *J. Am. Chem. Soc.* **1992**, *114*, 1990.
(15) Laibinis, P. E.; Bain, C. D.; Nuzzo, R. G.; Whitesides, G. M. *J. Phys. Chem.* **1995**, *99*, 7663.
(16) Dannenberger, O.; Weiss, K.; Himmel, H.-J.; Jäger, B.; Buck, M.; Wöll, Ch. *Thin Solid Films* **1997**, *307*, 183.
(17) Zharnikov, M.; Grunze, M. *J. Vac. Sci. Technol., B* **2002**, *20*, 1793.
(18) Chapman, R. G.; Ostuni, E.; Takayama, S.; Holmlin, R. E.; Yan, L.; Whitesides, G. M. *J. Am. Chem. Soc.* **2000**, *122*, 8303−8304.
(19) Chidsey, C. E. D.; Loiacono, D. N. *Langmuir* **1990**, *6*, 682.
(20) Sato, Y.; Ye, S.; Haba, T.; Uosaki, K. *Langmuir* **1996**, *12*, 2726.
(21) Esplandiu, M. J.; Hagenström, H.; Kolb, D. M. *Langmuir* **2001**, *17*, 828.
(22) Wacker, D.; Weiss, K.; Kazmaier, U.; Wöll, Ch. *Langmuir* **1997**, *13*, 6689.
(23) Köhn, F. Diploma Thesis, Universität Heidelberg, Heidelberg, Germany, 1998.
(24) Heister, K.; Zharnikov, M.; Grunze, M.; Johansson, L. S. O. *J. Phys. Chem. B.* **2001**, *105*, 4058.
(25) Schaible, M.; Petersen, H.; Braun, W.; Koch, E. E. *Rev. Sci. Instrum.* **1989**, *60*, 2172.
(26) Bernstorff, S.; Braun, W.; Mast, M.; Peatman, W.; Schröder, T. *Rev. Sci. Instrum.* **1989**, *60*, 2097.
(27) Wirde, M.; Gelius, U.; Dunbar, T.; Allara, D. L. *Nucl. Instrum. Methods Phys. Res., Sect. B* **1997**, *131*, 245.
(28) Jäger, B.; Schürmann, H.; Müller, H. U.; Himmel, H.-J.; Neumann, M.; Grunze, M.; Wöll, Ch.; *Z. Phys. Chem.* **1997**, *202*, 263.
(29) Heister, K.; Zharnikov, M.; Grunze, M.; Johansson, L. S. O.; Ulman, A. *Langmuir* **2001**, *17*, 8.
(30) Moulder, J. F.; Stickle, W. E.; Sobol, P. E.; Bomben, K. D. In *Handbook of X-ray Photoelectron Spectroscopy*; Chastian, J., Ed.; Perkin-Elmer Corp.: Eden Prairie, MN, 1992.
(31) Wagner, C. D.; Riggs, W. M.; Davis, L. E.; Moulder, J. F.; Muilenberg, J. E. *Handbook of X-ray Photoelectron Spectroscopy*; Perkin-Elmer Corp.: Eden Prairie, MN, 1979.
(32) Shirley, D. A. *Phys. Rev. B* **1972**, *5*, 4709.
(33) Wertheim, G. K.; Butler, M. A.; West, K. W.; Buchanan, D. N. E. *Rev. Sci. Instrum.* **1974**, *45*, 1369.
(34) Stöhr, J. *NEXAFS Spectroscopy*; Springer Series in Surface Science 25; Springer- Verlag: Berlin, 1992.
(35) Zharnikov, M.; Frey, S.; Heister, K.; Grunze, M. *Langmuir* **2000**, *16*, 2697.
(36) Batson, P. E. *Phys. Rev. B* **1993**, *48*, 2608.
(37) Nuzzo, R. G.; Zegarski, B. R.; Dubois, L. H. *J. Am. Chem. Soc.* **1987**, *109*, 733.
(38) Himmelhaus, M.; Gauss, I.; Buck, M.; Eisert, F.; Wöll, Ch.; Grunze, M. *J. Electron Spectrosc. Relat. Phenom.* **1998**, *92*, 139.
(39) Thome, J.; Himmelhaus, M.; Zharnikov, M.; Grunze, M. *Langmuir* **1998**, *14*, 7435.
(40) Bagus, P. S.; Weiss, K.; Schertel, A.; Wöll, Ch.; Braun, W.; Hellwig, C.; Jung, C. *Chem. Phys. Lett.* **1996**, *248*, 129.
(41) Väterlein, P.; Fink, R.; Umbach, E.; Wurth, W. *J. Chem. Phys.* **1998**, *108*, 3313.
(42) Weiss, K.; Bagus, P. S.; Wöll, Ch. *J. Chem. Phys.* **1999**, *111*, 6834.
(43) Outka, D. A.; Stöhr, J.; Rabe, J. P.; Swalen, J. D. *J. Chem. Phys.* **1988**, *88*, 4076.
(44) Hähner, G.; Kinzler, M.; Thümmler, C.; Wöll, Ch.; Grunze, M. *J. Vac. Sci. Technol., A* **1992**, *10*, 2758.
(45) Hähner, G.; Kinzler, M.; Wöll, Ch; Grunze, M.; Scheller, M. K.; Cederbaum, L. S. *Phys. Rev. Lett.* **1991**, *67*, 851; *Phys. Rev. Lett.* **1992**, *69*, 694 (erratum).
(46) Bierbaum, K.; Kinzler, M.; Wöll, Ch.; Grunze, M.; Hähner, G.; Heid, S.; Effenberger, F. *Langmuir* **1995**, *11*, 512.
(47) Witte, G.; Weiss, K.; Jakob, P.; Braun, J.; Kostov, K. L.; Woell, Ch. *Phys. Rev. Lett.* **1998**, *80*, 121.
(48) Ågren, H.; Carravetta, V.; Vahtras, O.; Pettersson, L. G. M. *Chem. Phys. Lett.* **1994**, *222*, 75.
(49) Hitchcock, A. P.; Brion, C. E. *J. Electron Spectrosc. Relat. Phenom.* **1979**, *15*, 201.
(50) Hitchcock, A. P.; Tronc, M.; Modelli, A. *J. Phys. Chem.* **1989**, *93*, 3068.
(51) Kinzler, M.; Schertel, A.; Hähner, G.; Wöll, Ch.; Grunze, M.; Albrecht, H.; Holzhüter, G.; Gerber, Th. *J. Chem. Phys.* **1994**, *100*, 7722.
(52) Walczak, M. M.; Chung, C.; Stole, S. M.; Widrig, C. A.; Porter, M. D. *J. Am. Chem. Soc.* **1991**, *113*, 2370.
(53) Engquist, I.; Lestelius, M.; Liedberg, B. *Langmuir* **1997**, *13*, 4003.
(54) Harder, P.; Allara, D. L.; Frey, S.; Shaporenko, A.; Zharnikov, M. Unpublished results.
(55) Preliminary results of the infrared absorption spectroscopy experiments, which will be published elsewhere, show that the average tilt angle of alkyl chains in NC-C16/Ag is equal to 25°.
(56) Preliminary results of the infrared absorption spectroscopy experiments, which will be published elsewhere, show that the average tilt angle of the CN group in NC-C16/Ag is equal to 68°.
(57) Fenter, P.; Eisenberger, P.; Li, J.; Camillone, N., III; Bernasek, S.; Scoles, G.; Ramanarayanan, T. A.; Liang, K. S. *Langmuir* **1991**, *7*, 2013.
(58) Fenter, P.; Eisenberger, P.; Liang, K. S. *Phys. Rev. Lett.* **1993**, *70*, 2447. Fenter, P.; Eberhardt, A.; Eisenberger, P. *Science* **1994**, *266*, 1216.
(59) Camillone, N.; Chidsey, C. E. D.; Liu, G.-Y.; Scoles, G. *J. Chem. Phys.* **1993**, *98*, 3503.
(60) Lampert, A. Ph.D. Thesis, Universität Heidelberg, Heidelberg, Germany, 1997.